Journal of Multidisciplinary Engineering Science and Technology (JMEST)
ISSN: 2458-9403
Vol. 3 Issue 12, December - 2016

Computational Simulation: Selected Applications In Medicine, Dentistry, And Surgery

R A J Wain[1,2], D Hammond[1], M McPhillips[1], A Fsadni[1] & J P M Whitty[1]
[1]Computational Medical Mechanics Group, University of Central Lancashire, Preston, PR1 2HE, UK.
Email: richwain@doctors.org.uk
[2]Institute of Translational Medicine, University of Birmingham, Birmingham, B15 2TT , UK.

***Abstract*—This article presents the use of computational modelling software (e.g. ANSYS) for the purposes of simulating, evaluating and developing medical and surgical practice. We provide a summary of computational simulation modelling that has recently been employed through effective collaborations between the medical, mathematical and engineering research communities. Here, particular attention is being paid to the modelling of medical devices as well as providing an overview of modelling bone, artificial organs and microvascular blood flows in the machine space of a High Performance Computer (HPC).**

Keywords: ***Computational simulation; Finite element analysis; Computational fluid dynamics; Bone; Dentistry; Blood flow; Microvascular; Lung; Heart; Bladder***

I. INTRODUCTION

This article presents the use of computational modelling software (e.g. ANSYS) for the purposes of simulating, evaluating and developing medical and surgical practice. In formative years the use of such specialist multi-physics engineering simulation software was deemed as the purview of highly experienced and qualified engineers. However, due in no small part to the wealth of training material made available (ANSYS customer portal), and the user friendly interface created by the vendors, in recent years, it has become sensible to expose clinicians to the power of computational simulation tools in order to inform medical and surgical practices. We provide a summary of computational simulation modelling that has recently been employed through effective collaborations between the medical, mathematical and engineering research communities. Here, particular attention is being paid to the modelling of medical devices as well as providing an overview of modelling bone and artificial organs in the machine space of a High Performance Computer (HPC). The article is by no means meant to be an authoritative account of computational medical modelling methods; the reader being directed to the extensive body of work from Professors Gibson (most notably Finite Element Analysis (FEA) of trabecular bone), and Steinman (Computational Fluid Dynamics (CFD) of physiological flows) for this. Therefore in the spirit of Prof. Steinman's recent review [1] it is hoped that the article will serve more to inspire new research questions, as well as provide a vehicle with which to describe on-going research in the authors' collaborative Computational Medical Mechanics Research group.

Generally computational modelling (particularly within the ANSYS and or CATIA software) consists of the discretisation of a geometrical domain, the physics of which is described by suitable continuum mechanics. The continuum Partial Differential Equations (PDE) which are solved generally subdivides the modelling disciplines into Structural (dominated by Finite Element Methods (FEM)), Fluids (dominated by Computational Fluid Dynamics (CFD)), and a combination of these loosely referred to as Fluid Structural Interaction (FSI) modelling. Such multi-physics simulation approaches allow solution of problems from a wide variety of environments including the industrial engineering, motorsport and medical fields, amongst others. In essence, all approaches have a centralised theme in that they attempt to solve, to varying degrees of accuracy, a particular field of interest, usually displacement, velocity, temperature or a combination of these in the aforementioned multi-physics problems.

II. FINITE ELEMENT BONE MODELLING

Finite element modelling has been used for over 40 years to simulate the way in which particular bones respond to stress and impact. Fracture patterns can be analysed, and the response of specific fracture fixation methods to wear and/or impact can be investigated. More recently, patient-specific geometries have been created with measured bone densities to give a more accurate representation of the response of bone to an external force in live patients.

The fundamental principles of FEM are essentially an extension of the Ritz method as introduced by Courant [2], which involves the minimization of functionals formulated though variational calculus. The term Finite Element was probably penned by Turner et al. [3] whom generalized the previous method described to a continuum geometrical domain so that stiffness and deflexion of different shaped structures could be effectively analysed. In essence, a geometric domain is discretized in to a number of finite elements, referred to as a mesh, each being in adherence to the world famous equation [4]:

$$k_i = \iiint_{CV} \overrightarrow{B}[\mathbf{D}]\overrightarrow{B}^T dV$$

where k_i is the stiffness matrix of the individual element within the Finite Element (FE) mesh, [D] is the elastic coupling, usually taking the form of the compliance matrix, though may be adjusted depending on the continuum mechanics to be simulated, and $\vec{B}$ is a vector of shape-functions. The shape functions can be envisaged as salient interpolation functions used to effectively approximate the primary, or in some cases the secondary, solution field. In the case of the modelling methods described throughout this section, the matrix [D] takes the form of the Timoshenko beam stiffness matrix (which includes beam shearing effects) for cellular solid models (trabecular bone §§2A) and the full anisotropic classical elastic compliance matrix (compact bone §§2B). Some of the salient details of current research practices will be outlined in the remainder of this section.

A. Trabecular bone modelling

Cellular solids are known to exist in many natural forms including wood, cork [5], trabecular (cancellous) bone [6] and even in the human skull, as shown in Figure 1 [5, 6]. They are also examples of natural sandwich panel composite materials. The mechanical response and micro-structural features of cellular solids are reasonably well understood and can be investigated using honeycomb and foam theories [7]. Honeycomb structures consist of repeated arrays of polyhedral cells [6] and are referred to as two-dimensional cellular solids. Foams are three-dimensional analogues of honeycombs and exist in open, with solid only at the edges of the polyhedra [5], or closed, with solid membranes over the faces of the polyhedra [8] forms.

One of the most influential works on analytical modelling of honeycombs was conducted by Gibson et al. [9]. This work is concerned with the in-plane mechanical properties of conventional foam structures (e.g. Figure 2). Much of the ground breaking research investigating the static performance and mechanical properties of cellular solid systems was conducted by Gibson and Ashby [6], in the mid-to-late 1980s, including analytical and FE modelling approaches. The primary deformation mechanism of trabecular bone systems has been shown to be rib flexure [9, 6]. Moreover, Gibson and Ashby's analytical model [6] has been extended to incorporate other minor deformation mechanisms such as stretching and hinging of the cell walls [10, 11]. These analytical modelling methods are incredibly effective in predicting the mechanical and failure properties of two-dimensional cellular systems in pristine forms. In addition, they are easily extended to three-dimensional analogues. However analytical techniques are less effective, with the notable exception of Smith et al. [12], in the prediction of such properties, when cellular systems contain defects i.e. missing ribs. In the main, analysis of defective cellular systems uses numerical finite element methods. Gibson and Ashby formalized the flexure model [9] in what has now become the classic treatise of the properties of cellular solids [6].

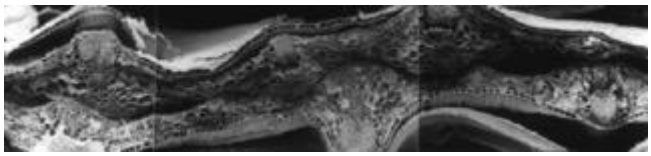

(a)

(b)

Figure 1. Examples of cellular bone (a) Trabecular bone, (b) Human skull (sources [5,6])

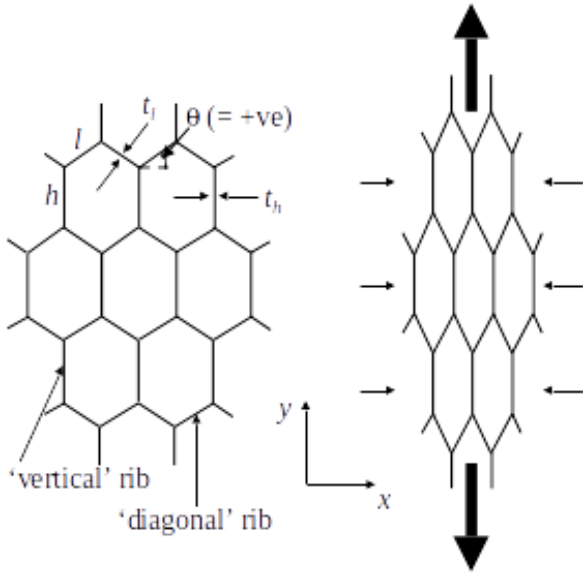

(a) Conventional honeycomb

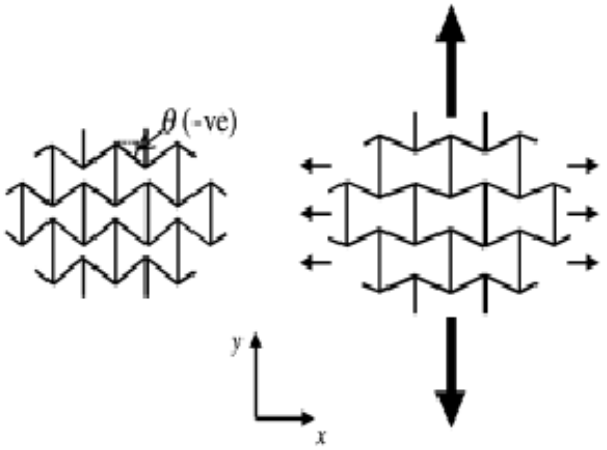

(b) Auxetic honeycomb

Figure 2. Two-dimensional trabecular bone models (a) Conventional honeycomb, (b) Auxetic honeycomb

A further important related area of research is the development of novel cellular materials that possess negative Poisson's ratios, the so-called auxetic materials [13]. These materials get broader in cross section when a tensile load is applied and conversely become thinner when compressed. Since the Poisson's ratio (ν_{xy}) is defined as the ratio of contractile strain to extensive strain when a material is under tensile loading, then for auxetic materials the so-called contractile strain is in fact tensile, leading to a realization of negative Poisson's ratios. In most cases, auxetic materials have been formed by alteration of the internal microstructure of a conventional material. For example, Figure 2 (a) shows a conventional two-dimensional trabecular bone unit cell, which could deform by hinging (say) of the walls. This would lead to elongation of the cell along any tensile loading direction, but would undergo contraction at right angles to any applied load; hence this unit cell has a positive ν_{xy}. However, if the geometry is modified so that cells adopt the re-entrant geometry shown in Figure 2 (b), then they elongate both along and transverse to the tensile loading direction, giving rise to novel auxetic behaviour. Two-dimensional honeycomb foams have been produced using silicone rubber or aluminium; such structures are elastically anisotropic [9]. However, the current interest in auxetics emerged in 1987 with the development of isotropic three-dimensional auxetic foams by Prof. Lakes at the University of Iowa [14]. Moreover, Lakes has found that auxetic foams are more resilient than non-auxetics, when exposed to fatigue loading conditions. Due primarily to the inability to measure the mechanical properties of bone in-situ, there has been no clear evidence within the literature that trabecular bone is auxetic. Moreover, bone tends to die before any accurate measurements can be made of the elastic properties using more traditional testing methods. However, due to their proven fatigue added resilience, these materials are still of great interest particularly in design of implantable prostheses.

There is evidence in the literature that changing the microstructure of cellular solids so they are inherently auxetic renders improvement of their dynamic (and acoustic) properties. However to date, there seems a distinct lack of literature detailing mathematical modelling and simulation of such properties. Where the static performance of cellular solids is concerned, three regions of strain dependent static stress have been identified [6]; these being, Linear elastic, Plateau Stress and Plastic. The primary and secondary regions were shown to be recoverable as the plateau stress was attributed to elastic buckling of the ribs. The plateau is also present in the compression of three-dimensional cellular foams, where the deformation was observed in localized bands [6]. Static modelling attempts to accurately repeat the three stages of elastic behaviour using non-linear finite element solution procedures resident in commercial software (e.g. ANSYS, see Figure 4). It has been shown [6] that whatever the failure mode in compression, all types of trabecular bones will exhibit the three regions. However, the text reports [6] that when loaded in tension, elastic cellular materials will show an almost instant transition from the linear elastic to the plastic region. That is, no plateau stress is observed. Plastic trabecular model systems still show a plateau stress region between the elastic to plastic regions, though it is considerably shorter. Brittle failure on the other hand shows no transition to the plastic region in tension and will appear to fail while still in the elastic region; a brittle failure is very abrupt in tension. Gibson and Ashby show that the type of bone fracture is dependent on the intrinsic material behaviour. That is, trabecular bone may react elastically or plastically depending on the nature of the intrinsic material. Furthermore, analytical and FE modelling has shown that if the trabeculae are constructed from a brittle material, failure of the whole structure exhibits brittle failure. As with any brittle solid, the fracture is controlled by the crack propagation, which can be calculated via fracture mechanics. This phenomenon has been proven using a novel crack propagation routine [10]. Recently our group has made one of the first attempts in Europe to employ mathematical modelling approaches used extensively in the mechanical engineering domain in the bio-medical sector. We are in the process of designing biomaterials with a cellular structure to replace bones. For example, titanium foams are being considered as the main substitute materials for trabecular bone as their structures and properties are very similar to those of bones. Progressive failure of bone structures under shock loading conditions have been presented; utilizing a brittle crack propagation routine developed in-house (Figure 3), featuring sophisticated birth and death of finite elements. That is, the progressive deactivations (death) of elements from the finite element models are used to simulate bone fracture. On the other hand the reactivation (birth) is used to simulate healing processes. The results show that under shock-loading conditions, the bone structures investigated here undergo catastrophic failure where a rapid reduction in the elastic modulus and both tensile and compressive strength properties is apparent.

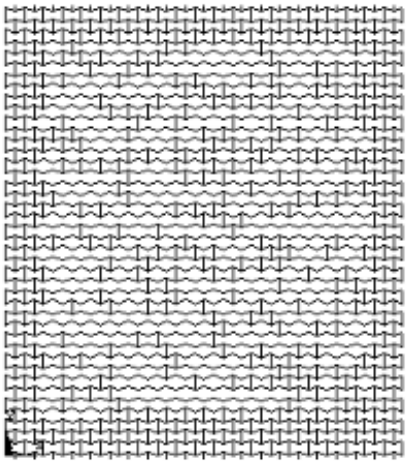

(a) Auxetic-diseased bone

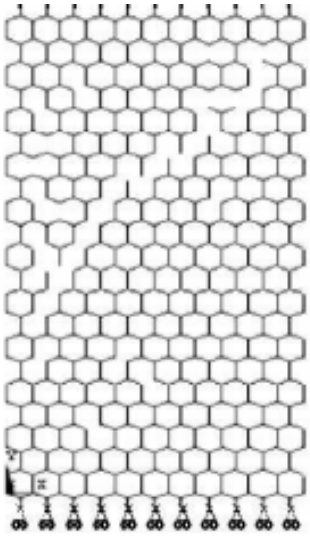

(b) Conventional fractured bone

Figure 3. Microstructural trabecular bone models (a) Auxetic-diseased, (b) Conventional fractured bone

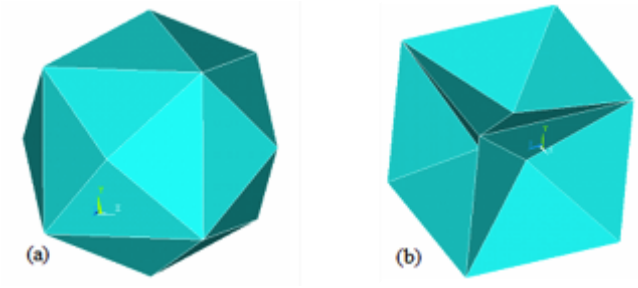

Figure 4. Three-dimensional models of finite elements

This research has progressed to investigate these phenomena more closely from a mathematical viewpoint by developing both analytical (continuum mechanical) and finite element modelling protocols to investigate the effect of the mechanical properties and failure modes in cellular systems with intrinsic brittle, ductile (elastic-plastic) and viscoelastic properties.

B. Cortical bone modelling

Surprisingly, due to the composite nature of compact bone, research in this area is still very much in its infancy with approximately 800 academic papers reported[3] in the last three decades. One of the earliest uses of the FEA method in prediction of mechanical properties of cortical bone dates back to 1991. Faulkner [15] created FEA models from quantitative computed tomographic patient data with and without osteoporosis. Simulation loads were applied to the vertebral models to estimate strength. Yield strength in the models from patients with osteoporosis was 570kPa ± 260kPa, at the 99.9% confidence level, which was shown to be some 28% lower than normal bone [15]. This rather rudimentary modelling was quite revolutionary in that it was probably the first time the strength and elastic properties of cortical bone had been predicted using FEA. The work is however an extension of the fundamental work performed on trabecular bone (§1A) and research in the dental community most notably Cook et al. [16] whom used three-dimensional FEA to determine the effect of implant elastic modulus on stresses in tissues around Low Temperature Isotropic (LTI) carbon and aluminium oxide dental implants. Models were constructed to represent a baboon mandible containing a blade type dental implant. It was shown that the use of LTI carbon and aluminium oxide dental implants as an abutment in a fixed bridge resulted in a reduction of stresses in tissues around the natural tooth when compared to nominal physiological stress levels. A three-unit fixed bridge was modelled connecting the dental implant to a natural molar. The results of the study indicated a three-fold reduction in stress in the crestal region when aluminium oxide implants were employed in comparison with carbon implant counterparts [16]. Since the FEA work within the dental and maxillofacial surgical communities is obviously most developed dating back to over a decade further than most of the rest of the medical community [17] the proceeding sub-sections will discuss these details further. The modelling procedure usually begins with rudimentary verification using extended Timoshenko beam theory [18] together with classical fracture mechanics similar to shown in Figure 5, where CATIA (Computer Aided Three-dimensional Interactive Application) was used to effectively confirm that, as expected, stress was significantly increased without the presence of the third molar [17]. These results have been subsequently verified using the separate commercially available and complimentary FE code ANSYS, and an analytical model developed in-house [19].

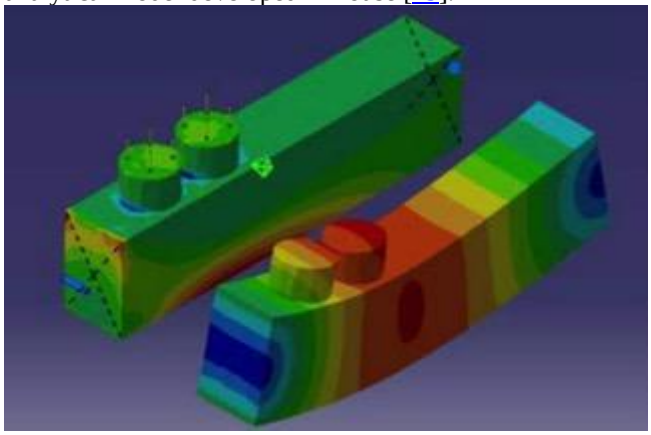

Figure 5. Rudimentary mandible showing areas of stress and strain

C. Dental applications

Goel et al. [20] investigated the stresses arising at the Dentino-Enamel Junction (DEJ) during function and noted that the shape of the DEJ was different under working cusps than non-working cusps. The results of this study showed that tensile stresses were elevated toward cervical enamel and also that mechanical inter-locking between enamel and dentin is weaker in the cervical region than in other areas of the tooth making it susceptible to crack.

Many studies have been carried out to assess the behaviour of teeth under occlusal load using FEA. Rees [21, 22] used this concept to estimate the effect of repeated loading on the restoration of cervical cavities. It was suggested that continual occlusal loading produced displacements and stresses under the buccal cervical enamel and dentin, increasing crack initiation and encouraging loss of restoration. This suggests that lingual walls of teeth should be equally susceptible to cervical wear as are buccal walls, but this is not supported by clinical findings where lingual surface lesions are comparatively rare. Further FEA studies by these authors showed that exposed dentine could be eroded by acid undermining enamel causing more breakdown and increased wear [22, 23]. Coelho et al. [24] conducted another study to test the hypothesis that micro-tensile bond strength values are inversely proportional to dentine-to-composite adhesive layer thickness through laboratory mechanical testing and FEA. They showed that single bonds were more effective than Clearfill self-etch adhesive system. Furthermore Kim et al. [25] compared the stress distribution during simulated root canal shaping and estimated the residual stress thereafter for some nickel-titanium rotary instruments using a 3D finite-element code, taking into account the non-linear mechanical behaviour of the nickel-titanium material. They concluded that the original Protaper design showed the greatest pull in the apical direction and the highest reaction torque from the root canal wall, whereas Profile showed the least. In Protaper, stresses were concentrated at the cutting edge and the residual stress reached a level close to the critical stress for phase transformation of the material. The residual stress was highest in Protaper followed by Protaper Universal and Profile.

Finite element analysis can be applied in three areas of Orthodontics, viz.

- Analysis of the skeleton,
- Design of orthodontic devices,
- Analysis of growth, remodelling and degeneration.

Orthodontic tooth movement can be achieved by assessing the remodelling of the alveolar bone (Figure 6). This is triggered by changes in the stress/strain distribution in the periodontium. FEM can be used to describe the stress situation within the Perio-Dontal Ligament (PDL) and surrounding alveolar bone. It can also be used as a tool to

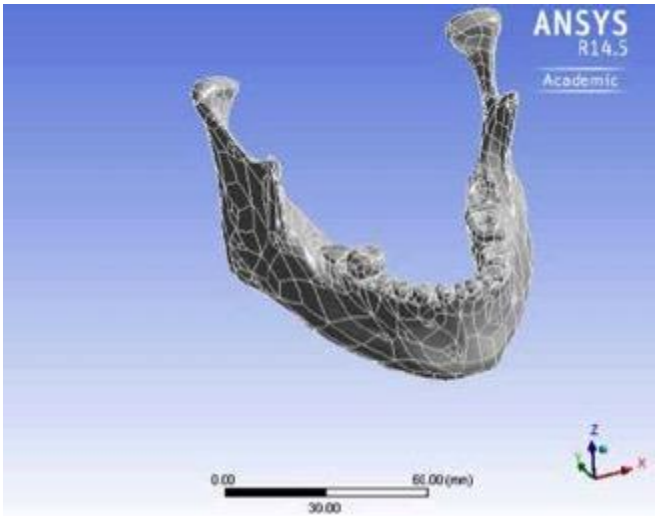

Figure 6. ANSYS alveolar and cortical bone meshes

study orthodontic tooth movement [26]. FEA has been a useful tool for morphometric analysis in craniofacial biology too. The Cephalometric Finite Element Analysis (CEFEA) code incorporates the advanced features of FEM though bypasses much of the technical details of the method. The code uses the colour graphics display akin to an FE post-processor to show size change, shape change, and angle of maximum change. These are pictured as coloured triangles of clinically relevant regions between pre- and mid- or post treatment lateral head films. The effect of altering the geometry of the bracket base mesh on the quality of orthodontic attachment employing a three-dimensional finite element computer model is another application of the method in orthodontics as discussed by Knox et al. [27]; here a CAD/CAM template gives orthodontists a safe way to place mini-screws [28].

D. Oral and maxillofacial trauma

In maxillofacial trauma computational simulation has been used for:

- Impact analysis,
- Optimal localisation of different osteosynthesis devices,
- Analysis of loads across a fracture.

Three-dimensional Computer-Aided-Design (CAD) models were generated simulating ten skulls [29]; impacts being simulated in an orbital region of these models in four specific patterns.

Pattern-1: All the energy works to cause the hydraulic effect.

Pattern-2: Two-thirds of the energy works to cause the hydraulic effect; one-third of the energy works to cause the buckling effect.

Pattern-3: One-third of the energy works to cause the hydraulic effect; two-thirds of the energy works to cause the buckling effect.

Pattern-4: The entire energy quantum works to cause the buckling effect.

Using the finite element method, the regions where fractures were theoretically expected to occur were calculated and compared with the aforementioned four patterns. This showed more fracture damage occurred for Pattern 1 than Pattern 2, and for Pattern 3 than for Pattern 4. This demonstrates that hydraulic and buckling mechanisms interact with one another. When these two mechanisms are combined, the orbital walls tend to develop serious fractures. Three-dimensional finite element models simulating atrophic mandibular fractures were constructed [30]. The models were divided into 4 groups according to plate thickness (1.0, 1.5, 2.0, and 2.5 mm). Fractures were simulated in left mandibular bodies, and 3 locking screws were used on each side of each fracture for fixation. Large-profile (2.0-mm-thick) locking plates showed better biomechanical performance than did 1.0- and 1.5-mm-thick plates, and can be considered an alternative reconstruction plate for the treatment of Class III atrophic mandibular fractures. In orthognathic surgery different osteotomy designs have been analysed, to see which osteotomy has the best biomechanical profile [30]. There is also work which has been performed on modelling soft tissues of the face with regards to orthognathic surgery outcomes [31]. Work is now progressing such that patient-specific CT imaging data can be imported in to the ANSYS FEA code using the open-source 3D-slicer[4] software (Figure 6). This will enable much more detailed clinically relevant modelling to be performed in the not so distant future [19]; with preliminary results being shown in Figure 7.

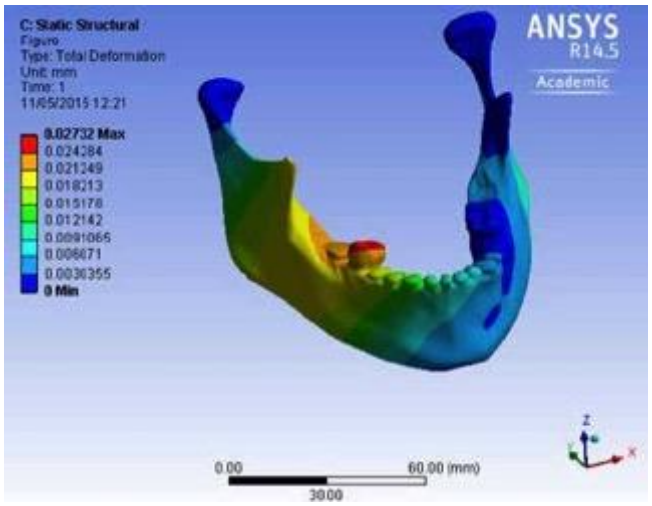

Figure 7. Preliminary finite element model results

E. Orthopaedic implants

This appears to be one of the largest fields of dental research involving finite element analysis. Pesqueiria et al. [32] wrote an excellent review article, which covers some of the complexity of the implant/dental interface. The mechanism of stress distribution and load transfer to the implant/bone interface is a critical issue affecting the success rate of implants. They reviewed the literature with reference to stress analysis methods associated with implant-supported prosthesis loading, and discussed their contributions in the biomechanical evaluation of oral rehabilitation with implants. It was found that several studies have used experimental (including photoelasticity, strain gauges), analytical and computational models by means of finite element analysis [33], to critically evaluate the biomechanical behaviour of dental implants. Consequently, FEA has been used to evaluate new components, configurations, materials and shape of implants.

III. COMPUTATIONAL FLUID DYNAMICS FOR BLOOD FLOW SIMULATION

Computational Fluid Dynamics (CFD) is a method used to numerically solve a series of governing equations in order to accurately predict resulting flow fields at specific parts of the cardiovascular system. Here CFD, with the correct blood physical properties assigned within the respective code, is used for numerical experimentation [34]. The greatest advantage of CFD is the ability to simulate flow and create numerical results in situations where experiments would be expensive and time-consuming, or in those circumstances that would be impossible to recreate experimentally. The potential for inaccurate or erroneous results however is great, particularly as this software is widely available and can be run on most domestic computers. It is therefore of utmost importance that numerical models are validated and verified. In addition a thorough understanding of fluid mechanics, and application of CFD to appropriate problems, is necessary to help to ensure realistic and reliable results.

Much of the groundbreaking work in this area has been conducted by Prof. Steinman's[5] team at the University of Toronto. Under his leadership the team have produced more than 250 academic papers over the past decade. The early work culminated in the development of the most impressive Vascular Modelling Toolkit (VMTK[6]) which effectively allows the production of three-dimensional geometrical surfaces models, interpolated from Digital Imaging and Communications in Medicine (DICOM) data. The use of the software is now rapidly becoming the pre-protocol to three-dimensional vascular model construction or CFD meshing algorithms. Prof. Steinman is currently focusing predictive modelling of the rupture of cerebral aneurysms, turbulence in blood flow as well as the development of an interactive ultrasound training simulator and flow visualization. As mentioned previously Steinman's opening chapter [1] to the text [35] detailing the necessary assumptions and their respective validity to haemodynamics is most informative and does provide some very valuable insights in to the state of the science over the last couple of decades or so. However, a more detailed, though earlier review, of the use of CFD for the exploration of haemodynamics is given elsewhere [36]. It is therefore

not the purpose of this section to revisit the work described by Prof. Steinman in his multiple treatise on the topic; more to provide an overview of the work of the authors in the context of CFD modelling of smaller blood vessels, particularly arteries.

A. Evolution of CFD for haemodynamics

Flow modelling and computing have been extensively used to develop a detailed understanding of local blood flow patterns since the link between altered blood vessel haemodynamics and the formation of atherosclerosis was made in the 1980s by Friedman et al. [37]. In the early 1990s, CFD emerged as a technique for investigating local flow patterns in extreme detail, making more sophisticated studies possible [38, 39]. Additionally, Perktold [40, 41, 42, 43] and colleagues were responsible for the majority of the novel work in this field, and were the first group to demonstrate the carotid bifurcation using CFD. The increasing availability of CFD as a research tool, combined with ever-improving computer capabilities, led to a multitude of studies into the local haemodynamic flow within vessels. Factors such as low wall shear stress [44], flow disturbance [45], high oscillatory shear stresses [46], and vessel wall tension [47] were all implicated as factors affecting atheroma formation through the use of CFD. These correlations are supported by studies carried out in animal models by DePaola et al. [48] who demonstrated that large shear stress gradients could induce morphological and functional changes in the endothelium in regions of disturbed flow.

As well as developments within CFD, significant improvements were also being made within medical imaging. This led to in vivo measurements of haemodynamics using techniques such as Doppler ultrasound [49], Magnetic Resonance Imaging (MRI) [50], and angiography [51]. It then became possible to combine CFD with image-based techniques to investigate realistic vascular geometries [52, 53, 54]. Detailed reviews of the developments of image-based modelling of blood flow over the last two decades have been carried out by Steinman [55] and Taylor [56].

In the early days of CFD, simulations initially required several days of computer processing and could only produce two-dimensional models of idealised geometries. Now however, it is possible to convert detailed high-quality medical images into complex three-dimensional meshes for simulation of blood flow in individualised patients [57]. This process involves contrast-enhanced Magnetic Resonance Imaging (ceMRI) of the vessels and the application of a computational filter to calculate flow rates. The ceMRI images are converted into a mesh and then a patient specific flow simulation is created using a CFD solver. Although these simulations are clinically relevant and can be used to aid therapeutic decision making for certain pathologies, for example aortic dissection, some limitations still exist. These are primarily related to assumptions made in order to reduce processing time of large volumes of information, including arterial wall non-slip conditions, rigid walls, and blood as a Newtonian fluid. This said, the extent to which these assumptions actually influence accuracy of the results is a subject of great debate, and one which is addressed eloquently and comprehensively by Steinman [58]. Our group is also exploring the influence of Newtonian / non-Newtonian properties on flow in small vessels [59] .

Application of CFD to blood flow within vessels, whether pristine or pathological, is complex, but the addition of a surgical procedure, such as a vascular anastomosis, creates further issues for consideration including compliance mismatch, new geometries and subsequently new local haemodynamics. Several studies have been carried out to simulate flow in a range of anastomoses both in large and small vessels and are outlined in detail in Migliavacca's review [60].

B. CFD for modelling microvascular anastomoses

There is little published work in this area, with only a few studies carried out to specifically investigate microvascular anastomoses using computational modelling. Al-Sukhun et al. [61] developed a finite element model (FEM) to study the effect of stress and strain in microvascular anastomoses. The principal finding of this study was that size discrepancy in an end-to-end anastomosis demonstrated a significant reduction in blood flow compared to that in an end-to-side anastomosis. A more recent study by the same group has examined the effect of vascular wall compliance on displacement at the anastomotic site [62], with the major finding being that a 45^{o} angle of inset, for an end-to-side anastomosis, caused significantly less deformation at the anastomotic site and as such was deemed preferable.

A further study into the computational modelling of microvascular anastomoses was that of Rickard et al. [63] who investigated several techniques for anastomosis in arteries with size discrepancy. Four idealised end-to-end anastomotic techniques were modelled where the recipient artery was smaller. CFD simulations were performed to evaluate flow patterns and Wall Shear Stress (WSS) in the idealised anastomoses, with the 'wedge' technique demonstrating the least flow separation (Figures 8 & 9). These studies have evaluated the flow fields through idealised microvascular anastomoses in detail, but neither investigated local haemodynamics around sutures, or explored the flow patterns through coupling devices. It was for these reasons that our group began using CFD to examine the influence of microvascular sutures and coupling devices on anastomotic blood flow [64, 65, 66].

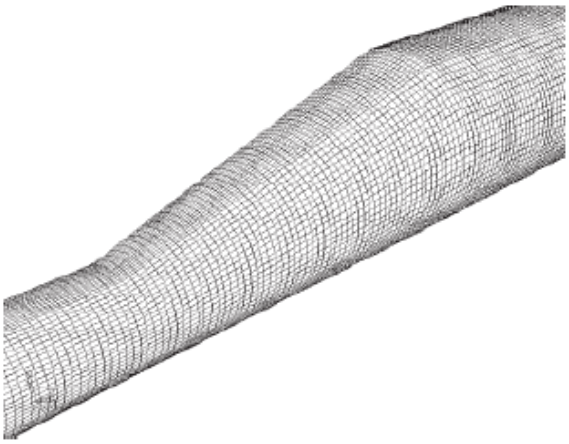

Figure 8. Geometry and mesh for the wedge microarterial anastomosis (source [63])

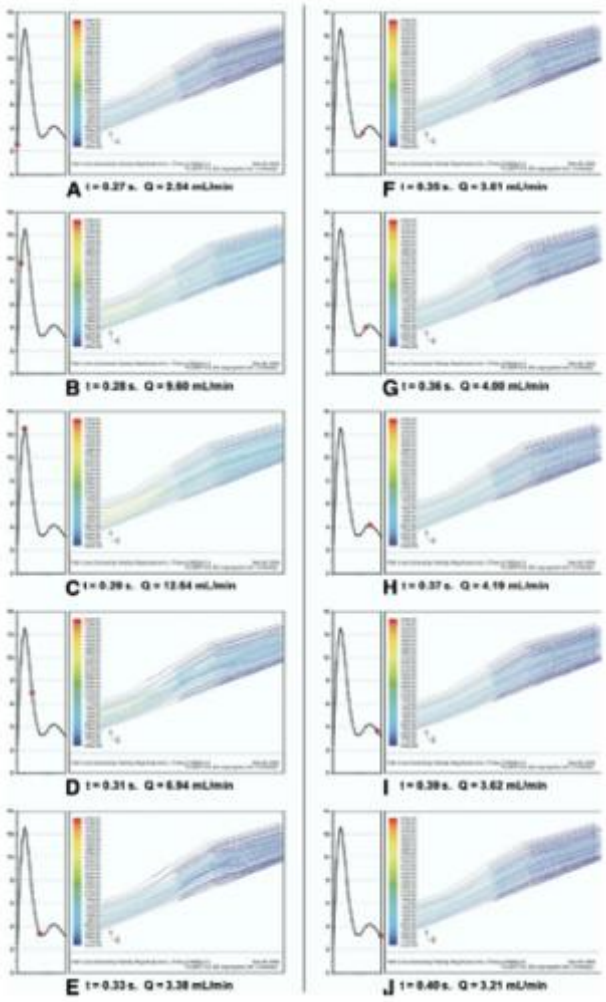

Figure 9. Demonstrating flow through the wedge microarterial anastomosis for vessels with size discrepancy (source [63])

C. Comparison of flow in idealised sutured and coupled microvascular anastomoses

Our first study used CFD to directly compare idealised sutured and coupled microvascular anastomoses to investigate the affect of each technique on intravascular blood flow [66]. Geometries of sutured and coupled anastomoses were created with dimensions identical to microvascular suture material and the GEM Microvascular Anastomotic Coupling (MAC) device using Computer Aided Design (CAD) and CFD software (Figures 10 & 11). Vessels were modelled as non-compliant 1mm diameter ducts, and blood was simulated as a Newtonian fluid. All analyses were steady-state and performed on arteries.

The simulations demonstrated less favourable flow properties in the sutured anastomosis when compared to those in the coupled model. Higher WSS and Shear Strain Rates (SSR) were found in the sutured technique (Figure 12), both of which are implicated in platelet activation and thrombus formation [67, 68, 69]. The sutured and coupled simulations were also compared to a pristine vessel, and interestingly the coupled anastomosis very closely matched the WSS and SSR profile seen in these pristine vessels. It could therefore be concluded, within the limits of an idealised study, that these observations demonstrate a theoretically more thrombogenic profile in a sutured anastomosis when compared to a coupled vessel [66].

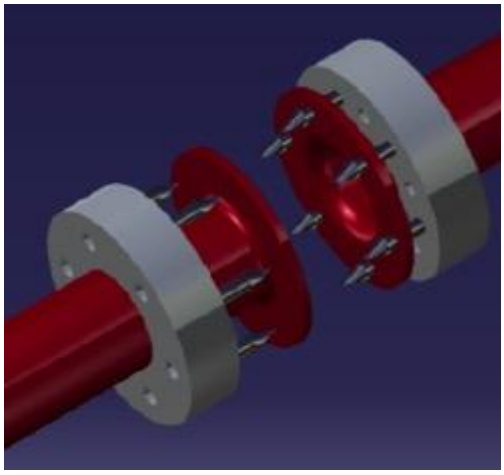

Figure 10. CAD coupler assembly (source [66])

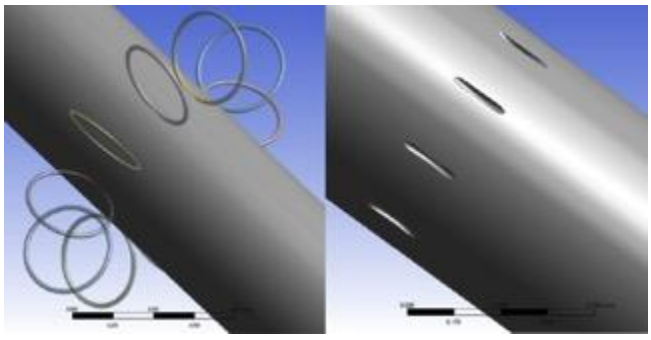

Figure 11. Idealised suture geometry creation using a subtraction body operation (source [66])

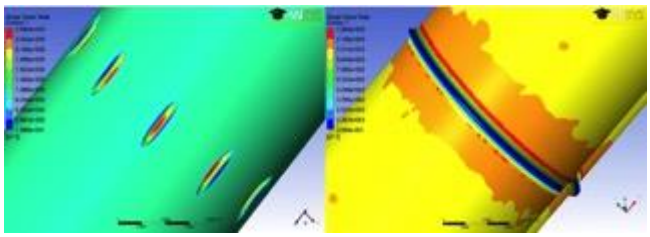

Figure 12. SSR distributions in the sutured (left) and coupled (right) anastomoses (source [66])

D. Flow analysis investigating realistic suture positioning in microarterial anastomoses

The natural progression of our comparative study was to create a sutured anastomosis geometry that more closely resembled clinical practice to ensure our previous findings were representative. The aim was to investigate the extent to which individual aspects of suture placement influence local haemodynamics within microarterial anastomoses [64]. Again, particular focus was placed on the WSS and SSR for each simulation. Measurements were taken from micrographs of sutured anastomoses in chicken femoral vessels, with each assessed for bite width, suture angle and suture spacing. Computational geometries were then created to represent the anastomosis. Each suture characteristic was parameterised to allow independent or simultaneous adjustment. Vessel simulations were performed in 2.5mm diameter ducts, again with blood as the working fluid. Consistently, vessel walls were simulated as non-compliant and a continuous Newtonian flow was applied, in accordance with current literature.

Suture bite angle and spacing had significant effects on local haemodynamics, causing notably higher local SSRs, when simulated at extremes of surgical practice (Figure 13). In keeping with our previous comparative study [66], these areas are potential sources of platelet activation and subsequent thrombus formation. A combined simulation, encompassing subtle changes of each suture parameter simultaneously i.e. representing optimum technique, created a more favourable SSR profile (Figure 14). As such, haemodynamic changes associated with optimum suture placement are unlikely to influence thrombus formation significantly. These findings support adherence to the basic principles of good microsurgical practice [64].

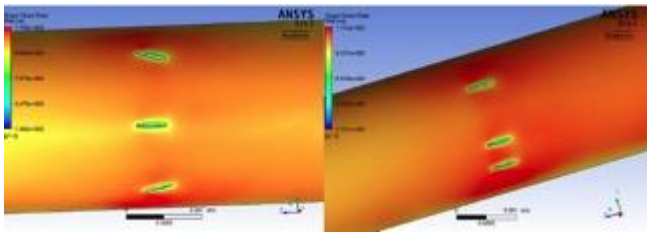

Figure 13. SSR distributions in sutured anastomoses with variation in suture angle (left) and spacing (right) (source [64])

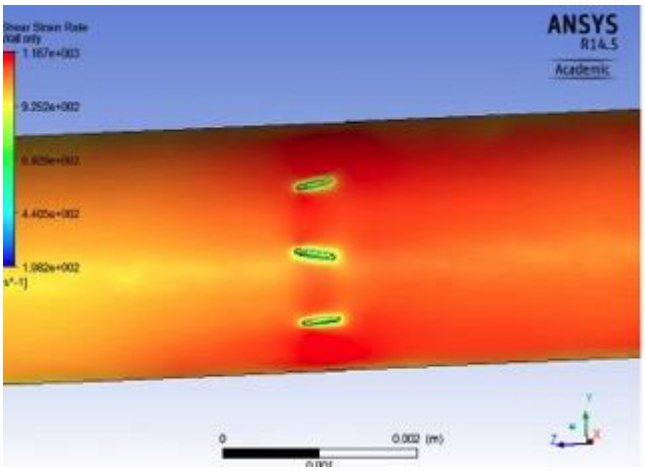

Figure 14. SSR distribution in sutured anastomosis with subtle variation in all parameters (source [64])

IV. SIMULATION OF ARTIFICIAL ORGANS

In recent years a number of rather successful attempts have been made to model the animal and human organs using engineering computational modelling software usually resident in a High Performance Computing (HPC) facility. Much of the early work, conducted in the mid-to-late 1990's, concentrated on the development of medical devices such as the mechanical heart valve (MHV) prostheses [70] in order to underpin more extensive experimental studies [71]. Such pioneering work was significantly extended over the next couple of decades and applied to other organs such as the lungs and bladder.

A. Heart models

As briefly mentioned previously, cardiovascular computational modelling began in the development of artificial heart valves [70]. This work combined experimental and computational data to investigate cavitation during the squeezing and rebounding phases of the closure of an Edwards-Duromedics (ED) MHV. CFD was employed to investigate a potential source of local erosion of the device and subsequent mechanical failure. The resultant simulation data demonstrated high flow velocities near the inflow surfaces of the valve leaflets which could produce cavitation within the flow fields. These corresponded with the areas of damage seen on explanted valves. One of the earliest uses of the commercial ANSYS-CFX software was performed by Song et al. [72] where a continuous flow ventricular assist device (VAD), a miniature centrifugal pump, was modelled for the first time. Here, stagnation points and vortices were used in order to imply possible sources of thrombosis.

During the last five years over 250 academic papers have been published pertaining to cardiovascular CFD modelling. Due in the main to heart decease persistently being one of the western worlds greatest killers, it continues to be the most rigorously applied medical CFD discipline. Many of these intensive studies involve the establishment of simulation boundary conditions. Such an approach has

been attempted on a couple of occasions by Khalafvand et al. [73, 74]. The latter study investigated the flow characteristics of a 48 year old male four months before surgery (Figure 15) in order to model benefits from a Surgical Ventricular Restoration (SVR) Coronary Artery Bypass Grafting (CABG) procedure. Vortex formation and development were presented in 3D geometry and also in 2D cross sections to demonstrate the size and location of crescent vortices in the left ventricle (LV). CFD was performed on models obtained from specific MRI scans acquired before (Figure 16) and after surgery (Figure 17). These results clearly demonstrated the flow patterns during diastole and systole, respectively. As wall dilatation continues, blood velocities across the mitral annulus increase, and vortices form underneath the aortic valve. These vortices became stronger and increased in length with increasing inlet velocity [74]. On the other hand, the flow patterns obtained from models after surgery show smaller vortices from close to the junction of the aortic root and left atrium.

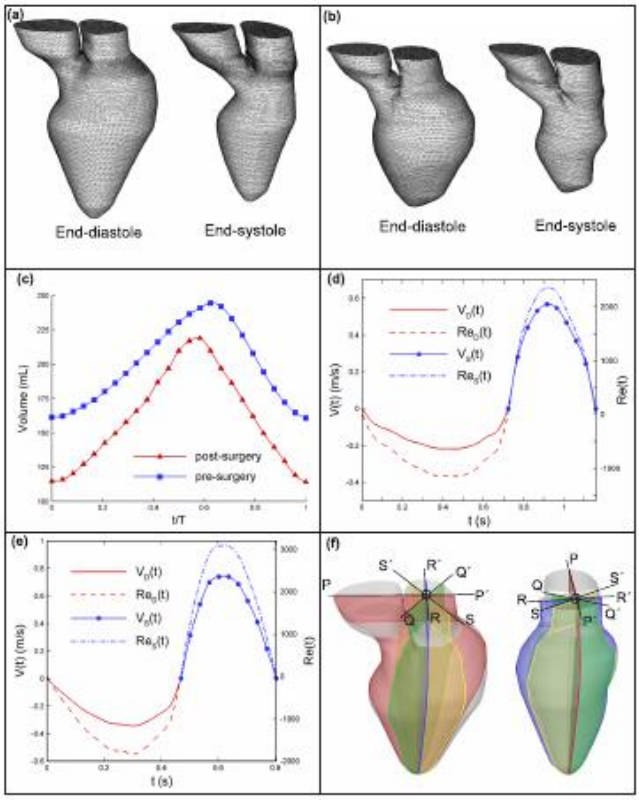

Figure 15. (a) Pre-surgery end-diastole and end-systole geometries, (b) post-surgery end-diastole and end-systole geometries, (c) temporary volume versus dimensionless time for before and after surgery LV , (d) temporary velocity versus time for pre-surgery LV , (e) temporary velocity versus time for post-surgery LV , and (f) four 2D longitudinal cross sections in two different views. $V_D(t)$ = velocity at the inlet during diastole; $V_S(t)$ = velocity at the outlet during systole; $Re_D(t)$ = Reynolds number at the inlet during diastole; $Re_S(t)$ = Reynolds number at the outlet during systole. (Source [75])

The derived pressure differences seen within the LV during diastole and systole, before and after surgery, clearly demonstrated the surgical efficiency. The pressure differences between ventricular base and apex after surgery are significantly increased and provide better LV filling and ejection. Maximum pressure differences were used as indices for assessing cardiac performance before and after the surgical procedure. The study clearly showed that SVR+CABG improves the performance of LV. It was therefore postulated that modelling different LV and valve diseases might well provide useful clinical applications [74].

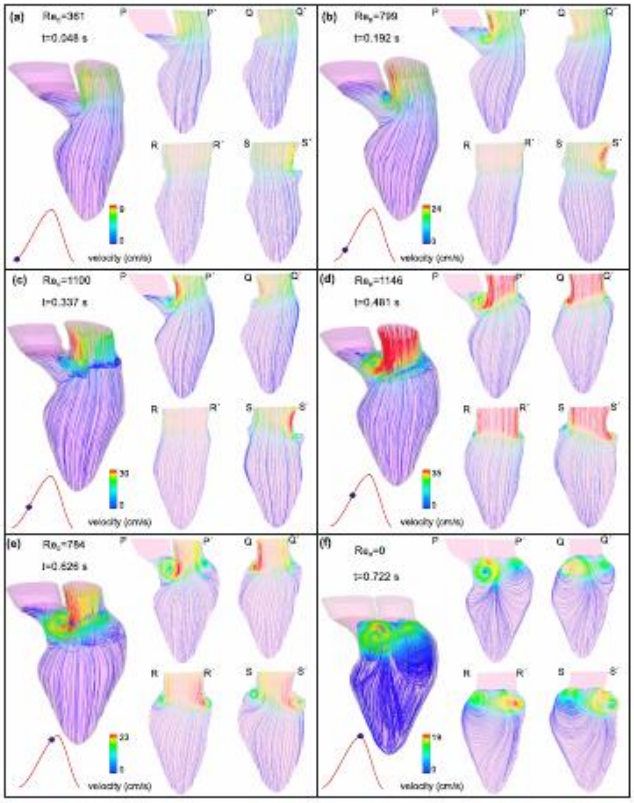

Figure 16. Flow patterns during diastole for before surgery at (a) t = 0.048[s], (b) t = 0.192[s], (c) t = 0.337[s], (d) t = 0.481[s], (e) t = 0.626[s], and (f) t = 0.722[s]. (Source [75])

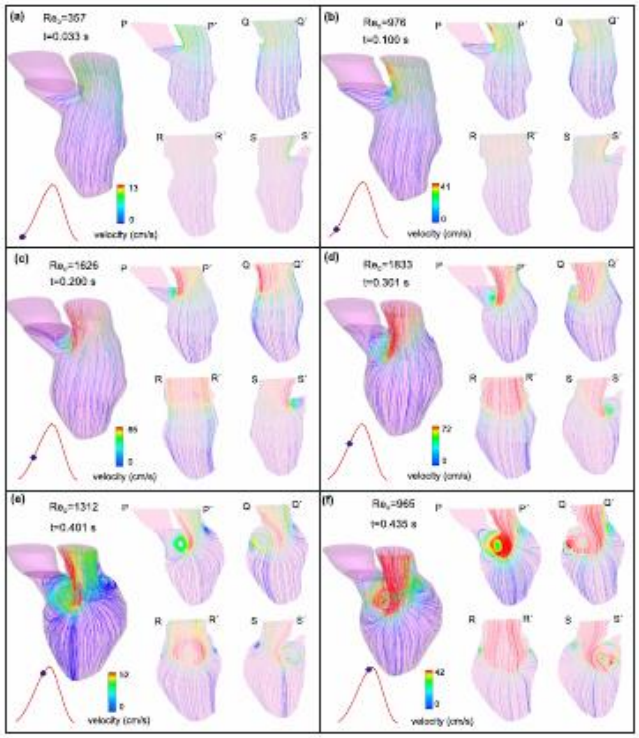

Figure 17. Flow patterns during diastole for after surgery at (a) t = 0.033[s], (b) t = 0.1[s], (c) t = 0.2[s], (d) t = 0.301[s], (e) t = 0.401[s], and (f) t = 0.435[s]. (Source [75])

CFD techniques are most widely reported throughout the journal of Artificial Organs, over the last five years some 68 articles have been dedicated to the work, which is some 75% greater than the next highest, i.e. Annals of Biomedical Engineering. For instance Kobayashi et al. [76] reported progressions made in the development of the Continuous-Flow Total Artificial Heart (Figure 18). The state-of-the art ANSYS-CFX commercial code was employed to model the right hydraulic output of an artificial heart having one motor and a rotating assembly supported by a hydrodynamic bearing. This work presents progress in four areas of development: the automatic speed control system, self-regulation to balance right/left inlet pressures and flows, haemolysis testing using calf blood, and coupled electromagnetics (EMAG) with the aforementioned CFD. Simulation results for a fixed rotor position, revealed little difference between the performance of the left, right, and bearing sections of the pump and that of the combined pump. These results were shown to be consistent with clinical expectations, as evidenced by flow-rates exchanged between pump sections along the connecting journal bearing flow path. The CFD analysis also revealed that the journal bearing pressure fields between the two pump sections provided the majority of the hydraulic radial force. These being established from a benchmarking study of nominal axial operations which were shown to move to more extreme conditions; location of the peak residence time within the fluid film of the hydrodynamic bearing were subsequently evaluated (Figure 19). Furthermore, the multi-physics coupled EMAG/CFD full pump solutions predicted hydraulic performance, static pressure taps throughout the pump, and rotor torque matched in vitro data. Additionally, axial force imbalances toward the left pump were found. Therefore the EMAG/CFD predicted the axial position of the rotating assembly in line with empirical data.

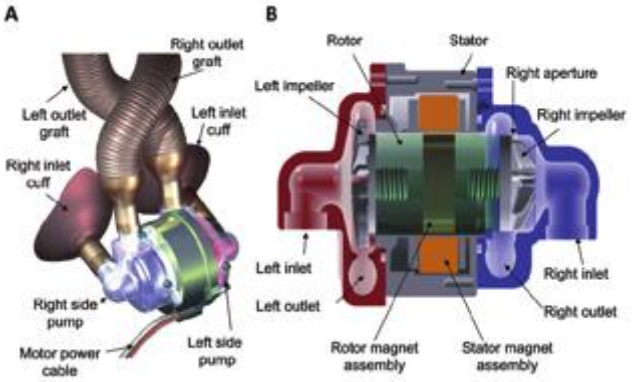

Figure 18. Image of CFTAH with (a) inflow cuff and outlet graft and (b) Cross section of the CFTAH. (Source [75])

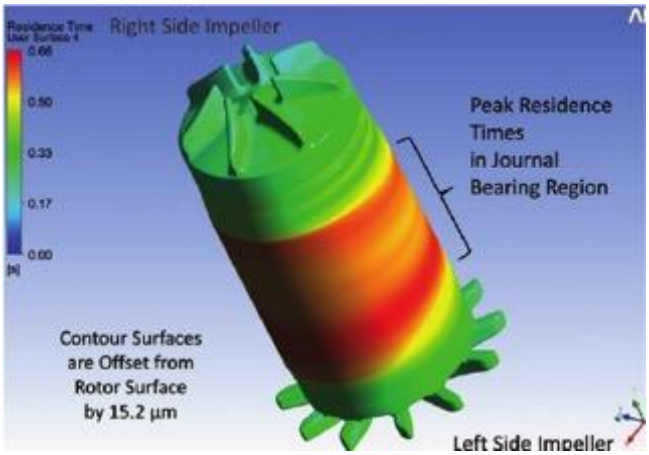

Figure 19. Peak resistance times in journal bearing region. (Source [75])

Recent reviews into the application of CFD for cardiovascular simulations have demonstrated use of medical image processing software to establish realistic three-dimensional models, e.g. [77, 78]. The review of Zhang et al. [77] details technological advancements outlining some of key ramifications of CFD modelling with regard to coronary artery disease research. Particular attention is being directed toward patient-specific modelling, with respect to geometry reconstruction, establishment of realistic boundary conditions, fluid–structure interaction and relationships between specific haemodynamic conditions and clinical indices. The use of CFD in assessing the viability of myocardium and suitability for percutaneous coronary intervention is also being explored.

B. Lung models

The complete, multi-scale geometry of airflow within human bronchopulmonary segments presents a great challenge to medical imaging and consequently, to two-dimensional and three-dimensional solid and surface modelling. Such modelling regimes are probably one of the key challenges in biomedical CFD. Nonetheless researchers have proposed reduced geometry models in which multiple airway paths (Figure 20) have been created. For instance,

Walters et al. [79] proposed a method for closing the CFD model by application of physiologically correct boundary conditions at truncated outlets. Realistic reduced geometric lung airway models based on CT data were constructed which included extrathoracic, bronchial, and bronchiolar regions. Results with respect to pressure drop through the airway using this new approach were shown to be in good agreement with more established ones. CFD simulation of airflow and particle concentration in a similar lung airway model have been carried out by Liang et al. [80]. This study attempted to obtain accurate information on flow fields and particle deposition patterns in human lung airways using a rudimentary model (Figure 20). Particle tracking using the ANSYS-Fluent software showed that, for ultra fine particles, the geometrical structure of the lung airway model was the dominant factor affecting the flow fields and particle deposition throughout the lungs. Furthermore, simulations of particle deposition were shown to be mostly affected by local airflow velocities. The work also skilfully demonstrated that just under 50% of the particles were deposited at the mouth, with about 12% of the particles being deposited in the so-called Generation-0 section the model (Figure 20). The result of this simplified modelling process could be employed to investigate the principal factors influencing the air velocity distributions and particle deposition. Such simulation data should be useful in the design of delivery systems such as dry powder inhalers.

Numerical simulations were conducted under normal breathing frequency and high-frequency oscillatory ventilation (HFOV) conditions using user-defined C-programs together with CFD code ANSYS-Fluent. Two-dimensional and three-dimensional double bifurcating lung models were created, and the geometry based on the Weibel's pulmonary model analogous to those of Liang et al. [80] i.e. Figure 20. Simulations were carried out to study the air flow fields, gas transportation, and wall shear stresses in the airways for different Reynolds numbers (i.e. Re = 400 and 1000) and several respiratory cycle frequencies. The numerical models successfully reproduced a number of results observed empirically [81].

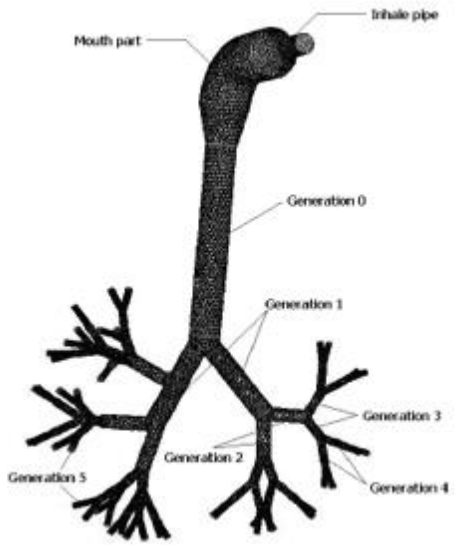

Figure 20. Configuration of the lung airway mode (Source [80])

C. Bladder models

Computational simulation in the urinary system has been employed to investigate the mechanical properties of the ureter, specifically the hydrodynamics of flow along a distensible tube with peristaltic motion [82]. In addition, models of the lower urinary tract have been proposed including those for examining bladder function and neural control [83].

The works of Niu & Chang [84] and Pok et al. [85] have explored the lower urinary tract in more detail, with special consideration given to the bladder. The first of these works details preliminary CFD simulations of the lower urinary system. Here, suitable assumptions are provided which simplifies the lower urinary geometry to a rigid body. The ANSYS-CFX commercial code is used to evaluate the urine flow velocity distributions, and wall pressure, ergo wall shear stress. Simulation results showed an increased inflow-rate due in the main to intense secondary flows occurring at the end of the urethra. A phenomenon which was accompanied by oscillating pressure fields and wall shear stress distributions at peak flow rates [84].

The study by Pok et al. [85] investigated a bio-reactor suitable for human bladder regeneration. The CFD simulations incorporated porous regions, nutrient consumption for smooth muscle cells (SMCs) and effective diversities in to the modelling protocols. Steady state simulations with different inlet shapes were simulated similar to those shown in Figure 21 [85]. These virtual approach capabilities allowed for the integrating mass and momentum transfer calculations in a single system therefore outlining problems which may have arisen from scaling-up the reactors.

As mentioned previously, probably due to the natural multi-physics involved, the literature with regard to CFD or indeed FEA of mammal (including human) bladders is not particularly numerate. A related area of research is that of tissue engineering where it was stated that: "CFD modeling helps characterize fluid flow, provides initial estimates, and more importantly supplements experimental results. Influence of parameters such as velocity, oxygen tension, stress, and strain on tissue growth can be effectively studied throughout the reactor using CFD". Patrachari et al. [33]

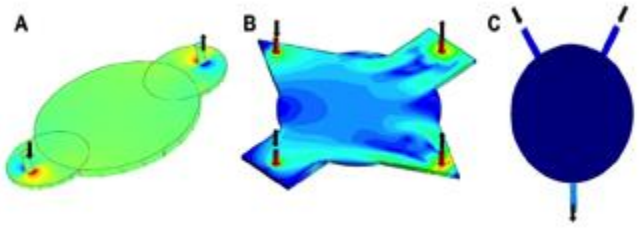

Figure 21. Different bioreactor configurations tested using CFD computations (A) Circular bioreactor containing a and scaffold optimized for uniform stress distribution. (B) Circular bioreactor containing a diameter scaffold with two inlets and two outlets. Also inlet and outlet shapes are

different. (C) Spherical bioreactor with features resembling human bladder. (Source [86])

SUMMARY

This article provides an overview of several specific areas within medicine, dentistry and surgery where computational simulation has been used to evaluate or develop the respective fields. We have described principal techniques involved with the finite element method for bone modelling, and explored the development of this for evaluating dental implants and predicting fracture propagation. Details of computational fluid dynamics have been discussed in the context of blood flow simulation, along with the specifics of microvascular flows and the incorporation of anastomotic technique. Lastly, the place of computation in the creation of artificial organs has been presented, particularly in the context of cardiorespiratory and urinary systems.

As previously discussed, the intention of this article is not to be all-encompassing, but more a précis to demonstrate the broad range of applications of computational simulation, and its subsequent potential to influence and improve treatment for patients.

ACKNOWLEDGMENTS

The authors wish to express their thanks to Dr. David Smith from the School of Mathematics, University of Birmingham for his advice and critique in the compilation of this manuscript.

FUNDING

This research did not receive any specific grant from funding agencies in the public, commercial, or not-for-profit sectors.

R A J Wain is currently a Research Fellow funded by the Institute of Translational Medicine, University of Birmingham.

CONFLICT OF INTEREST STATEMENT

All authors declare they have no conflict of interest

REFERENCES

[1] D.A. Steinman. Assumptions in modelling of large artery hemodynamics. Modeling, Simulation and Applications , 5:1–18, 2012.
[2] R. Courant. Variational methods for the solution of problems of equilibrium and vibrations. Bulletin American Mathematical Society , 49(2):165–172, 1943. 187.
[3] M. J. Turner, R. W. Clough, H. C. Martin, and L. P. Topp. Stiffness and deflection analysis of complex structures. Aerospace science and technology, 23:805–823, 1956.
[4] O. C. Zienkiewicz and R. L. Taylor. The Finite Element Method. Butterworth-Heinemann, Oxford, sixth edition, 2005.
[5] L.J. Gibson. Biomechanics of cellular solids. Journal of Biomechanics , 38(3):377–399, 2005.
[6] Lorna J Gibson and Michael F Ashby. Cellular solids: structure and properties. Cambridge university press, 1997.
[7] M.J. Silva and L.J. Gibson. Modeling the mechanical behavior of vertebral trabecular bone: Effects of age-related changes in microstructure. Bone, 21(2):191–199, 1997.
[8] J.P.M. Whitty, B.Henderson, P. Myler, and C. Chirwa. Crash performance of cellular foams with reduced relative density part 1: Rib thickness variation. International Journal of Crashworthiness , 12(6):677–688, 2007.
[9] L.J. Gibson, M.F.Ashby, G.S. Schajer, and C.I. Robertson. Mechanics of two dimensional cellular solids. Proceedings of The Royal Society of London, Series A: Mathematical and Physical Sciences , 382(1782):25–42, 1982.
[10] J.P.M. Whitty, A. Alderson, P. Myler, and B. Kandola. Towards the design of sandwich panel composites with enhanced mechanical and thermal properties by variation of the in-plane poisson's ratios. Composites Part A: Applied Science and Manufacturing , 34(6):525 – 534, 2003. {ICMAC} 2001 - International Conference for Manufacturing of Advanced Composites.
[11] I.G. Masters and K.E. Evans. Models for the elastic deformation of honeycombs. Composite Structures, 35(4):403–422, 1996.
[12] C.W Smith, J.N Grima, and K.E Evans. A novel mechanism for generating auxetic behaviour in reticulated foams: missing rib foam model. Acta Materialia , 48(17):4349 – 4356, 2000.
[13] Ken E Evans. Auxetic polymers: a new range of materials. Endeavour, 15(4):170 – 174, 1991.
[14] R. Lakes. Negative poisson's ratio materials [8]. Science , 238(4826):551, 1987.
[15] K.G. Faulkner, C.E. Cann, and B.H. Hasegawa. Effect of bone distribution on vertebral strength: Assessment with patient-specific nonlinear finite element analysis. Radiology , 179(3):669–674, 1991. cited By 149.
[16] S.D. Cook, J.J. Klawitter, and A.M. Weinstein. The influence of implant elastic modulus on the stress distribution around lti carbon and aluminum
oxide dental implants. Journal of Biomedical Materials Research,15(6):879–887, 1981. cited By 29.
[17] D. Hammond and J. Whitty. Finite element analysis and dentistry. Faculty Dental Journal , 6(3):134, 2015.
[18] J. M. Gere and S. P. Timoshenko. Stength of materials. PWS Pub Co., 1997.
[19] D. Hammond. biomechanics of the human mandible with and without the third moalar . PhD thesis, Medicine and Dentistry, Univeristy of Central Lancashire, 2016.
[20] V. K. Goel, S. C. Khera, L. Ralson, and K. H. Chang. Stresses at the dentino-enamel junction of human teeth: A finite element investigation. Journal of Prosthetic Dentistry, 66(4):451–459, 1991.
[21] J.S. Rees. The role of cuspal flexure in the development of abfraction lesions: a finite element study. European Journal of Oral Sciences ,106(6):1028, December 1998.
[22] J.S. Rees and P.H. Jacobsen. The effect of cuspal flexure on a buccal class v restoration: a finite element

study. Journal of Dentistry , 26(4):361 – 367,1998.
[23] J.S. Rees. The effect of variation in occlusal loading on the development of abfraction lesions: A finite element study. Journal of Oral Rehabilitation , 29(2):188–193, 2002.
[24] P.G. Coelho, C. Calamia, M. Harsono, V.P. Thompson, and N.R.F.A. Silva. Laboratory and fea evaluation of dentin-to-composite bonding as a function adhesive layer thickness. Dental Materials , 24(10):1297–1303, 2008.
[25] H.-C. Kim, G.S.-P.Cheung, C.-J. Lee, B.-M. Kim, J.-K. Park, and S.-I. Kang. Comparison of forces generated during root canal shaping and residual stresses of three nickel-titanium rotary files by using a three-dimensional finite-element analysis. Journal of Endodontics , 34(6):743–747, 2008.
[26] P. M. Cattaneo, M. Dalstra, and B. Melsen. The finite element method:
a tool to study orthodontic tooth movement. Journal of Dental Research , 84(5):428 – 433, 2005.
[27] J. Knox, B. Kralj, P. Hubsch, J. Middleton, and M.L. Jones. An evaluation of the quality of orthodontic attachment offered by single- and double-mesh bracket bases using the finite element method of stress analysis. Angle Orthodontist , 71(2):149–155, 2001.
[28] H. Liu, D.-X. Liu, G.Wang, C.-L.Wang, and Z.]Zhao. Accuracy of surgical positioning of orthodontic miniscrews with a computer-aided design and manufacturing template. American Journal of Orthodontics and Dentofacial Orthopedics , 137(6):728.e1–728.e10, 2010.
[29] H. Arbag, H. Korkmaz H, K. Ozturk, and Y. Uyar. What happens between pure and buckling mechanisms of blowout fractrues? journal of craniomaxillofacial surgery , 34(4):306–313, 2010.
[30] A. Vajgel, I. B. Camargo, R. B. Willmersdorf, T. Menezes de Melo, J. R. L. Filho, and R. J. de Holanda Vasconcellos. Comparative finite element analysis of the biomechanical stability of 2.0 fixation plates in atrophic mandibular fractures. Journal of Oral and Maxillofacial Surgery , 71(2):335– 342, 2013.
[31] H. Takahasji, Moriyama S, H. Furuta, H. Matsunga, Y. Sakamoto, and T. Kikuta. Three lateral osteotomy designs for bilateral saggital split osteotomy: Biomechanical analysis with finite element analysis. Head and Face Medicine , 26(6):4, 2010.
[32] A. A. Pesqueira, M. C. Goiato, and H.C. Filho. Use of stress analysis methods to evaluate the biomechanics of oral rehabilitation with implants. Journal of Oral Implantology , 40:217–228, 2014.
[33] S. Parameswaran, Z. Chen, Z. He, S. Parameswaran, R. Raj, and Y. Hu. Numerical simulations of high frequency respiratory flows in 2d and 3d lung bifurcation models. International Journal of Computational Methods in Engineering Science and Mechanics , 15(4):337–344, 2014.
[34] Amir Keshmiri and Kirstie Andrews. Vascular Flow Modelling Using Computational Fluid Dynamics. In Mark Slevin and Garry McDowell, editors, Handbook of Vascular Biology Techniques , pages 343–361. Springer Netherlands, 2015.
[35] D. Ambrosi, G. Rozza, and A. Quarteroni, editors. Modeling of Physiological Flows . Springer-Verlag Italia, 2012.
[36] D.A. Steinman. Image-based computational fluid dynamics: A new paradigm for monitoring hemodynamics and atherosclerosis. Current Drug Targets - Cardiovascular and Haematological Disorders , 4(2):183–197, 2004.
[37] M H Friedman, G M Hutchins, C B Bargeron, O J Deters, and F F Mark. Correlation between intimal thickness and fluid shear in human arteries. Atherosclerosis, 39(3):425–436, June 1981.
[38] X Y Xu and M W Collins. A review of the numerical analysis of blood flow in arterial bifurcations. Proceedings of the Institution of Mechanical Engineers. Part H, Journal of Engineering in Medicine , 204(4):205–216, 1990.
[39] C Kleinstreuer, S Hyun, J R Buchanan, P W Longest, J P Archie, and G A Truskey. Hemodynamic parameters and early intimal thickening in branching blood vessels. Critical Reviews in Biomedical Engineering , 29(1):1–64, 2001.
[40] K Perktold, H Florian, and D Hilbert. Analysis of pulsatile blood flow: a carotid siphon model. Journal of Biomedical Engineering , 9(1):46–53, January 1987.
[41] K Perktold and R Peter. Numerical 3d-stimulation of pulsatile wall shear stress in an arterial T-bifurcation model. Journal of Biomedical Engineering , 12(1):2–12, January 1990.
[42] K Perktold, R M Nerem, and R O Peter. A numerical calculation of flow in a curved tube model of the left main coronary artery. Journal of Biomechanics , 24(3-4):175–189, 1991.
[43] K Perktold, M Resch, and R O Peter. Three dimensional numerical analysis of pulsatile flow and wall shear stress in the carotid artery bifurcation. Journal of Biomechanics , 24(6):409–420, 1991.
[44] D N Ku, D P Giddens, C K Zarins, and S Glagov. Pulsatile flow and atherosclerosis in the human carotid bifurcation. Positive correlation between plaque location and low oscillating shear stress. Arteriosclerosis (Dallas, Tex.) , 5(3):293–302, June 1985.
[45] P E Hughes and T V How. Flow structures at the proximal side-to-end anastomosis. Influence of geometry and flow division. Journal of Biomechanical Engineering, 117(2):224–236, May 1995.
[46] M Ojha. Wall shear stress temporal gradient and anastomotic intimal hyperplasia. Circulation Research, 74(6):1227–1231, June 1994.
[47] M Hofer, G Rappitsch, K Perktold, W Trubel, and H Schima. Numerical study of wall mechanics and fluid dynamics in end-to-side anastomoses and correlation to intimal hyperplasia. Journal of Biomechanics, 29(10):1297–1308, October 1996.
[48] N DePaola, M A Gimbrone, Jr, P F Davies, and C F Dewey, Jr. Vascular endothelium responds to fluid shear stress gradients. Arteriosclerosis and Thrombosis: A Journal of Vascular Biology / American Heart Association , 12(11):1254–1257, November 1992.
[49] P R Hoskins. Quantitative techniques in arterial Doppler ultrasound. Clinical Physics and Physiological Measurement: An Official Journal of the Hospital Physicists' Association, Deutsche Gesellschaft Für Medizinische Physik and the European Federation of Organisations for Medical Physics , 11 Suppl A:75–80, 1990.
[50] N J Pelc, R J Herfkens, A Shimakawa, and D R Enzmann. Phase contrast cine magnetic resonance imaging.

Magnetic Resonance Quarterly , 7(4):229– 254, October 1991.
[51] O Smedby. Angiographic methods for the study of fluid mechanical factors in atherogenesis. Acta Radiologica. Supplementum , 380:1–38, 1992.
[52] David A Steinman. Image-based computational fluid dynamics modeling in realistic arterial geometries. Annals of Biomedical Engineering , 30(4):483– 497, April 2002.
[53] Armin Leuprecht, Karl Perktold, Sebastian Kozerke, and Peter Boesiger. Combined CFD and MRI study of blood flow in a human ascending aorta model. Biorheology , 39(3-4):425–429, 2002.
[54] Luca Antiga, Marina Piccinelli, Lorenzo Botti, Bogdan Ene-Iordache, Andrea Remuzzi, and David A Steinman. An image-based modeling framework for patient-specific computational hemodynamics. Medical & Biological Engineering & Computing, 46(11):1097–1112, November 2008.
[55] David A Steinman and Charles A Taylor. Flow imaging and computing: large artery hemodynamics. Annals of Biomedical Engineering, 33(12):1704–1709, December 2005.
[56] Charles A Taylor and David A Steinman. Image-based modeling of blood flow and vessel wall dynamics: applications, methods and future directions: Sixth International Bio-Fluid Mechanics Symposium and Workshop, March 28-30, 2008 Pasadena, California. Annals of Biomedical Engineering , 38(3):1188–1203, March 2010.
[57] Christof Karmonik, Jean Bismuth, Mark G Davies, and Alan B Lumsden. Computational fluid dynamics as a tool for visualizing hemodynamic flow patterns. Methodist DeBakey Cardiovascular Journal , 5(3):26–33, 2009.
[58] David A. Steinman. Assumptions in modelling of large artery hemodynamics. In Davide Ambrosi, Alfio Quarteroni, and Gianluigi Rozza, editors, Modeling of Physiological Flows , number 5 in MS&A — Modeling, Simulation and Applications, pages 1–18. Springer Milan, 2012.
[59] Justin P. M. Whitty, Richard A. J. Wain, Andrew Fsadni, Jules Simo, and Francis J. Computational non-newtonian hemodynamics of small vessels. J Bioinf Com Sys Bio , 1(1):103, 2016
[60] Francesco Migliavacca and Gabriele Dubini. Computational modeling of vascular anastomoses. Biomechanics and Modeling in Mechanobiology , 3(4):235–250, June 2005.
[61] Jehad Al-Sukhun, Christian Lindqvist, Nureddin Ashammakhi, and Heikki Penttilä. Microvascular stress analysis. Part I: simulation of microvascular anastomoses using finite element analysis. The British Journal of Oral & Maxillofacial Surgery , 45(2):130–137, March 2007.
[62] Jehad Al-Sukhun, Heikki Penttilä, and Nureddin Ashammakhi. Microvascular stress analysis: Part II. Effects of vascular wall compliance on blood flow at the graft/recipient vessel junction. The Journal of Craniofacial Surgery , 22(3):883–887, May 2011.
[63] Rory F Rickard, Chris Meyer, and Don A Hudson. Computational modeling of microarterial anastomoses with size discrepancy (small-to-large). The Journal of Surgical Research , 153(1):1–11, May 2009.
[64] Richard A. J. Wain, Justin P. M. Whitty, D Hammond, M McPhillips, and Waqar Ahmed. Microarterial anastomoses: a parameterised computational study examining the effect of suture position on intravascular blood flow. Microvascular Research, 105:141-148, 2016.
[65] Richard A. J. Wain. Computational modelling of blood flow through sutured and coupled microvascular anastomoses . Master of science, by research, University of Central Lancashire, April 2013.
[66] Richard A. J. Wain, Justin P. M. Whitty, Milind D. Dalal, Michael C. Holmes, and Waqar Ahmed. Blood flow through sutured and coupled microvascular anastomoses: a comparative computational study. Journal of plastic, reconstructive & aesthetic surgery: JPRAS , 67(7):951–959, July 2014.
[67] James J Hathcock. Flow effects on coagulation and thrombosis. Arteriosclerosis, thrombosis, and vascular biology , 26(8):1729–1737, August 2006.
[68] Feng Shen, Christian J Kastrup, Ying Liu, and Rustem F Ismagilov. Threshold response of initiation of blood coagulation by tissue factor in patterned microfluidic capillaries is controlled by shear rate. Arteriosclerosis, thrombosis, and vascular biology , 28(11):2035–2041, November 2008.
[69] G J Roth. Developing relationships: arterial platelet adhesion, glycoprotein Ib, and leucine-rich glycoproteins. Blood , 77(1):5–19, January 1991.
[70] D. Bluestein, S. Einav, and N.H.C. Hwang. A squeeze flow phenomenon at the closing of a bileaflet mechanical heart valve prosthesis. Journal of Biomechanics, 27(11):1369–1378, 1994.
[71] V.B. Makhijani, H.Q. Yang, A.K. Singhal, and N.H.C. Hwang. An experimental-computational analysis of mhv cavitation: Effects of leaflet squeezing and rebound. Journal of Heart Valve Disease , 3(SUPPL. 1):S35–S48, 1994.
[72] X. Song, H.G. Wood, and D. Olsen. Computational fluid dynamics (CFD) study of the 4th generation prototype of a continuous flow ventricular assist device (VAD). Journal of Biomechanical Engineering , 126(2):180–187, 2004.
[73] S.S. Khalafvand, E.Y.K. Ng, L. Zhong, and T.K. Hung. Fluid-dynamics modelling of the human left ventricle with dynamic mesh for normal and myocardial infarction: Preliminary study. Computers in Biology and Medicine , 42(8):863–870, 2012.
[74] S.S. Khalafvand, L. Zhong, and E.Y.K. Ng. Three-dimensional CFD/MRI modeling reveals that ventricular surgical restoration improves ventricular function by modifying intraventricular blood flow. International Journal for Numerical Methods in Biomedical Engineering , 30(10):1044–1056, 2014.
[75] M. Kobayashi, D. J. Horvath, N. Mielke, A. Shiose, B. Kuban, M. Goodwin, K. Fukamachi, and L. A. R. Golding. Progress on the design and development of the continuous-flow total artificial heart. Artificial Organs, 36(8):705–713, 2012.
[76] Mariko Kobayashi, David J Horvath, Nicole Mielke, Akira Shiose, Barry Kuban, Mark Goodin, Kiyotaka Fukamachi, and Leonard AR Golding. Progress on the design and development of the continuous-flow total artificial heart. Artificial organs, 36(8):705–713, 2012.
[77] J. Zhang, L. Zhong, B. Su, M. Wan, J. S. Yap, J. P. L.

Tham, L. P. Chua, D. N. Ghista, and R. S. Tan. Perspective on cfd studies of coronary artery disease lesions and hemodynamics: A review. International Journal for Numerical Methods in Biomedical Engineering , 30:659–680, 2014.

[78] N. Lee, M. D. Taylor, and R. K. Banerjee. Right ventricle-pulmonary circulation dysfunction: a review of energy-based approach. BioMedical Engineering OnLine , 14((Suppl 1):S8):12–20, 2015.

[79] D.K. Walters, G.W. Burgreen, D.M. Lavallee, D.S. Thompson, and R.L. Hester. Efficient, physiologically realistic lung airflow simulations. IEEE Transactions on Biomedical Engineering , 58(10):3016–3019, 2011.

[80] H. Liang, Y. Li, C. Zhang, and J. Zhu. Air flow and solid particle deposition patterns in a lung airway model. International Journal of Transport Phenomena , 10:277–291, 2008.

[81] Zixi Chen, Shamini Parameswaran, Yingying Hu, Zhaoming He, Rishi Raj, and Siva Parameswaran. Numerical simulations of high-frequency respiratory flows in 2d and 3d lung bifurcation models. International Journal for Computational Methods in Engineering Science and Mechanics , 15(4):337–344, 2014.

[82] Ghazaleh Hosseini, JJ Williams, Eldad J Avital, A Munjiza, D Xu, and James A Green. Computational simulation of urinary system. In San Francisco, USA: Proc World Congress Eng Comput Sci , 2012.

[83] CH Fry, P Sadananda, DN Wood, N Thiruchelvam, RI Jabr, and R Clayton. Modeling the urinary tract computational, physical, and biological methods. Neurourology and urodynamics , 30(5):692–699, 2011.

[84] Y. Niu and D. Chang. Cfd simulation of shear stress and secondary flows in uretha. Biomedical Engineering: Applications, Basis and Communications, 19(02):117–127, 2007.

[85] S. Pok, D. V. Dhane, and S.V. Madihally. Computational simulation modeling of bioreactor configurations for regenerating human bladder. Computer Methods in Biomechanics and Biomedical Engineering , 16(8):840– 851, 2013. PMID: 22224865.

[86] A. R. Patrachari, J. T. Podichetty, and S.V. Madihally. Application of computational fluid dynamics in tissue engineering. Journal of Bioscience and Bioengineering, 114(2):123–132, May 2012.